International Journal of Concrete Structures and Materials
Vol.10, No.4, pp.451–460, December 2016
DOI 10.1007/s40069-016-0163-6
ISSN 1976-0485 / eISSN 2234-1315

Prediction of Shear Strength for Large Anchors Considering the Prying Effect and Size Effect

Kangsik Kim[1,2),*], Kwangsoo Lee[3)], and Gyeonghee An[4)]

(Received March 9, 2016, Accepted July 2, 2016, Published online October 28, 2016)

Abstract: An anchorage system is necessary in most reinforced concrete structures for connecting attachments. It is very important to predict the strength of the anchor to safely maintain the attachments to the structures. However, according to experimental results, the existing design codes are not appropriate for large anchors because they offer prediction equations only for small size anchors with diameters under 50 mm. In this paper, a new prediction model for breakout shear strength is suggested from experimental results considering the characteristics of large anchors, such as the prying effect and size effect. The proposed equations by regression analysis of the derived model equations based on the prying effect and size effect can reasonably be used to predict the breakout shear strength of not only ordinary small size anchors but also large size anchors.

Keywords: large anchor, shear strength, CCD method, 45 degree cone method, bolt diameter, embedment depth, edge distance, prying effect, size effect.

List of Symbols

A_b	Area of the bottom surface
A_s	Area of the side surface
A_f	Area of the failure surface
c_1	Distance from the anchor to the edge of the concrete member
d_o	Diameter of the anchor
f_{ck}	Specified compressive strength of the concrete
h_{ef}	Effective embedment depth
l_e	The load-bearing length where $l_e = h_{ef}$ for anchors with a constant stiffness over the full length of an embedded section, and l_e will never exceed $8d_o$
l_f	Depth of failure surface
m_f	Load-magnification factor
P_1	Force applied to the anchor
P_2	Reaction force
P_3	Resultant force of P_1 and P_2
s_e	Relative strength
V_b	Shear strength of the anchor for breakout failure
$\psi_{c,V}$	Modification factor for concrete with no cracking

[1)]Department of Architectural Engineering, Hanyang University, Seoul 04763, Korea.

[2)]KEPCO RI, Daejeon 34056, Korea.

*Corresponding Author; E-mail: kimsudad@naver.com

[3)]Department of Architectural Engineering, Yeoju Institute of Technology, Yeoju 12652, Korea.

[4)]Korea Advanced Institute of Science and Technology, Civil & Environmental Engineering, Daejeon 34141, Korea.

1. Introduction

In most reinforced concrete structures, attachments like pipes, mechanical facilities and prefabricated components involve anchorage systems that are classified either as a cast-in-place system or a post-installed system. These anchorage systems always introduce concentrated loads to the concrete of structures. Anchorage systems resist tensile and shear loading either alone or together. Failure modes under tensile loading are steel tensile failure, pullout failure, concrete cone failure and so on. Failure modes under shear loading are also steel shear failure, concrete pryout failure, concrete breakout failure, etc.

The existing design codes for reinforced concrete structures, for example ACI 318 (2015), ACI 349 (2015), *fib*2010 (Federation Internationale du Beton (fib) 2013), etc. give the prediction equations for the strength of anchorage systems suggested by experimental and theoretical research results. These prediction equations, however, do still have some limitations, especially for large size anchors. For example, the equations can only be used for anchors with diameters of not more than 50 mm (2 in.) and effective embedment depths of not more than 635 mm (25 in.) in ACI 349-13 (2015). However, large anchors are frequently necessary in reinforced concrete structures such as containment buildings of nuclear power plants and turbine generator foundation of thermal power plants.

The purpose of this paper is to suggest a model for prediction of the shear strength of a large anchor failed by concrete breakout. Experiments on large anchors under shear loading are conducted. Prediction model is suggested based on the experimental results with consideration of the prying effect and the size effect.

2. Experiment with a Shear Anchor with a Large Diameter

2.1 Materials

Experiments on large anchors under shear loading are conducted following the standard in ASTM E-488 (1998). The shear load and displacement of the anchor are measured during the test. The test setup is shown in Fig. 1a.

The mixture proportion and compressive strength of the concrete are presented in Table 1. Ready-mixed concrete is used for the test and its compressive strength is between 35.3 MPa and 38.3 MPa. The compressive strength in Table 1 is the average strength of three cylindrical specimens of $\phi 100 \times 200$ mm in accordance with KS F 2405 (2010).

High strength anchor bolt in ASTM A 540 Class B (2005) is used. The head of the anchor consists of one thick round plate with two nuts in the upper and bottom parts of the plate for full resistance to the bearing force as shown in Fig. 1b. The material properties of anchor bolt are shown in Table 2.

2.2 Preparation of Specimen

The test variables, the anchor bolt diameter ($d_o = 63.5$, 76.2, 88.9 mm), the effective embedment depth ($h_{ef} = 635$, 762 mm), and the edge distance ($c_1 = 381$, 508, 762 mm), are shown in Table 3; the compressive strength of the concrete is fixed ($f_{ck} = 38$ MPa) even though the experimental values are a little scattered as shown in Table 1. A number and a test group are assigned to each specimen according to the test variables as shown in Table 3. 'VD', 'VH', and 'VE' stand for 'variable diameter', 'variable height', and 'variable edge distance'. Three to five specimens for each type are made according to ASTM E 488 (1998). The height of the specimens is longer than 1.5 times the effective embedment depth h_{ef} and the distance between the supporting points is longer than 3 times the edge distance c_1 as shown in Fig. 1b.

2.3 Experimental Results

2.3.1 Shear Strength

Figure 2 presents the load–displacement curve for each test anchor. The shear strengths from the test results are given in Table 3. The average value of the test results of

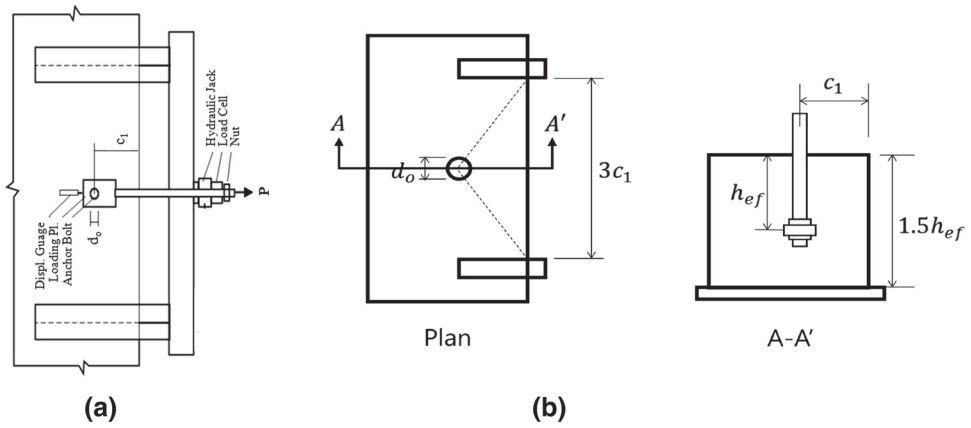

Fig. 1 Test setup and details of specimen. **a** Test setup. **b** Details of specimen.

Table 1 Mixture proportion and compressive strength of concrete.

Specimen no.	Mixture proportion								f_{ck} (MPa)
	W/B (%)	S/A (%)	kg/m^3						
			W	C	F	S	G	Ad.	
S1	42.4	44.0	171	302	101	740	986	2.82	37.5
S2	42.4	44.0	171	302	101	740	986	2.82	37.5
S3	42.4	44.0	171	302	101	740	986	2.82	38.3
S4	42.4	44.0	171	302	101	740	986	2.82	38.3
S6	36.7	41.8	184	426	75	658	959	3.01	35.3
S7	36.7	41.8	184	426	75	658	959	3.01	35.3

Table 2 Material properties of anchor bolt.

Standard	f_y (MPa)	f_u (MPa)	E_s (MPa)
ASTM A540 B23	960.4	1063.3	205,880

Table 3 Test variables and test results of each specimen.

Test group	Specimen no.	Concrete strength f_{ck} (MPa)	Anchor diameter d_0 (mm)	Anchor head		Embedment depth h_{ef} (mm)	Edge distance c_1 (mm)	V_{test} (kN) (a)	V_{aci} (kN) (b)	V_{ccd} (kN) (c)	Ratio	
				Dia. (mm)	Thk. (mm)						(a)/(b)	(a)/(c)
VD	S1	37.5	63.5	165	59	635	508	496.4	711.4	832.1	0.70	0.60
	S2	37.5	76.2	197	70	635	508	470.9	779.4	911.6	0.60	0.52
	S3	38.3	88.9	229	93	635	508	489.5	850.6	984.6	0.58	0.50
VH	S2	37.5	76.2	197	70	635	508	470.9	779.4	911.6	0.60	0.52
	S4	38.3	76.2	197	70	762	508	470.9	787.6	911.6	0.60	0.52
VE	S6	35.3	63.5	165	59	635	381	274.2	448.3	540.5	0.61	0.81
	S1	37.5	63.5	165	59	635	508	496.4	711.4	832.1	0.70	0.60
	S7	35.3	63.5	165	59	635	762	1046.4	1268.0	1528.7	0.83	0.68

each test specimen is indicated as 'V_{test}' and the predicted shear strength by Eq. (1) given in ACI 349-13 (2015), and the CCD method (Fuchs et al. 1995) results are indicated as 'V_{aci}' and 'V_{ccd}' in Table 3. ACI provides Eq. (1) for the uncracked section under a service load in SI units.

$$V_b = \psi_{c,V}\, 0.6\left(\frac{l_e}{d_o}\right)^{0.2}\sqrt{d_o}\sqrt{f_{ck}}(c_1)^{1.5} \tag{1}$$

where V_b is the shear strength of the anchor for breakout failure, $\psi_{c,V}$ is the modification factor for concrete with no cracking, l_e is the load-bearing length where $l_e = h_{ef}$ for anchors with a constant stiffness over the full length of an embedded section, and l_e will never exceed $8d_o$, d_o is the diameter of the anchor, f_{ck} is the specified compressive strength of the concrete, and c_1 is the distance from the anchor to the edge of the concrete member.

As shown in Table 3, the shear strength is overestimated by ACI code by more than 30 % and by CCD by more than 40 % for a large anchor. So a prediction model for shear strength in large anchor system is needed.

2.3.2 Failure Shape

The crack is propagated at about a 30° angle to the edge with an increasing shear displacement of the head of the anchor bolt after a shear load is applied to the large anchorage system (Lee et al. 2010). The angle of the crack is a little smaller than the 35° angle in a small anchorage system (ACI Committee 349 2015). All specimens experiences abrupt breakout failures when the cracks are reached the edge of the specimens. Figure 3 shows the crack mapping of each specimen.

2.3.3 Depth of Failure Surface, l_f

Figure 4 shows the failure shape of specimen S4 (d_o = 76.2 mm, c_1 = 508 mm, h_{ef} = 762 mm). According to the failure shape of the specimen S4, the depth of failure surface l_f is about $4d_o$ (356 mm). Shear loading applied to the anchor leads to a strain parallel to the loading and a crack orthogonal to the loading. The crack propagates toward the end of the anchor, and the breakout failure is started at a depth of failure surface which is about $4d_o$ (356 mm) for the specimen S4. The load is transferred through the upper part of anchor with length of l_f until the concrete is finally broken.

3. Derivation of the Equation for the Breakout Shear Strength of a Large Anchor

3.1 Area of Failure Surface

The failure cracking area of concrete under tensile loading as shown in Fig. 5a can be expressed as a function of the embedment depth of anchor h_{ef}. However, the cracking area of the concrete under shear loading in Fig. 5b is affected by the edge distance c_1, diameter d_o, and depth of failure surface l_f. The cracking area is not uniform through the edge distance. Figure 6 shows the failure shape roughly. The shape of the failure surface is actually round and curved, but

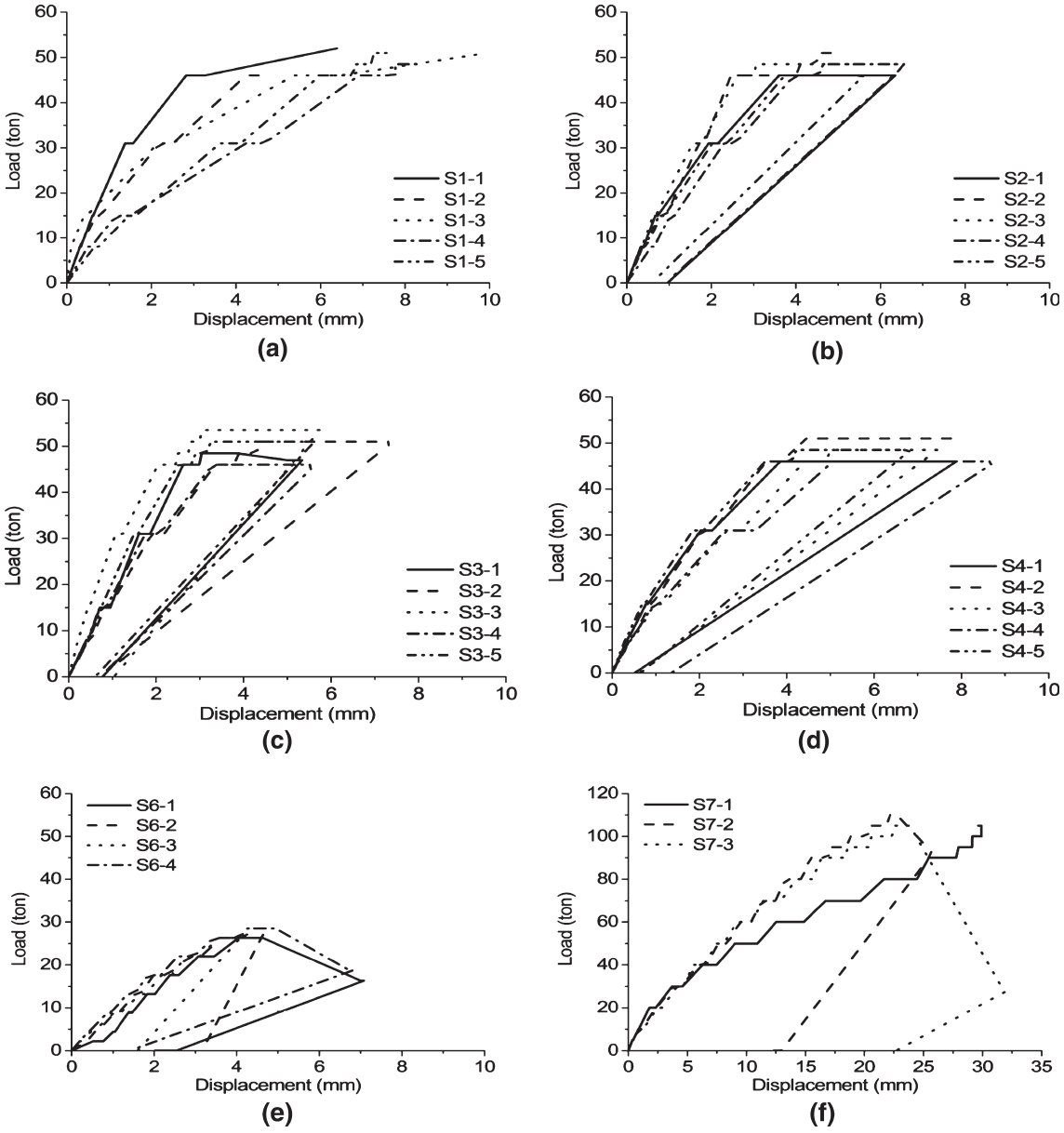

Fig. 2 Load–displacement curve of large anchors. **a** S1. **b** S2. **c** S3. **d** S4. **e** S6. **f** S7.

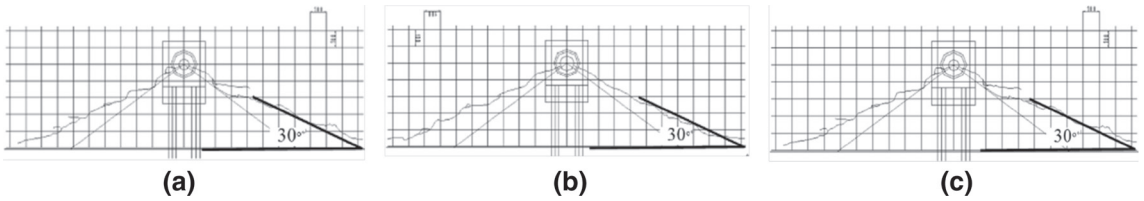

Fig. 3 Crack mapping. **a** VD. **b** VH. **c** VE.

the area of the failure surface A_f can be defined as Eq. (2) by assuming a curved surface to a flat one as shown in Fig. 6c.

$$A_f = A_b + A_s = m_1 c_1^2 + m_2 c_1 l_f \tag{2}$$

where A_b and A_s are the area of the bottom and side surface, respectively, m_1 and m_2 are empirical constants.

The bottom area of failure surface is proportional to the square of edge distance c_1, and the proportional constant m_1 is a function of crack angles θ_1 and θ_2. The side area is proportional to the product of the edge distance and the depth of failure l_f, and the constant m_2 depends on the flexural stiffness of the anchor, which is a function of the depth of failure l_f and diameter d_o as well as the angles θ_1 and θ_2. Equation (2) can be rewritten as Eq. (3) by considering the characteristic of constants m_1 and m_2.

$$A_f = m_1 c_1 \left[c_1 + m_3 \left(\frac{l_f}{d_o} \right)^{m_4} d_o^{m_5} \right] \tag{3}$$

where m_3, m_4 and m_5 are empirical constants.

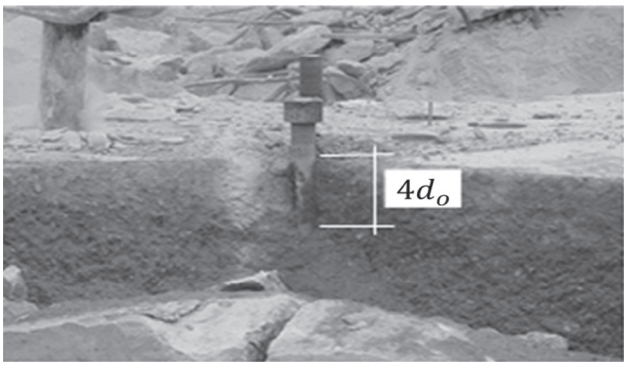

Fig. 4 Failure shape of front side (S4).

The failure surface area of concrete is actually a function of the edge distance c_1 and depth of failure l_f. However, Eq. (3) can be simplified as Eq. (4) which is the same form as suggested in ACI 349-13 (2015) without much error.

$$A_f = m_6 \left(\frac{l_f}{d_o}\right)^{m_7} d_o^{m_8} c_1^{m_9} \tag{4}$$

where m_6, m_7, m_8, and m_9 are empirical constants.

3.2 Size Effect

The size effect can be defined as follows: The resisting force per unit area of concrete decreases while the area increases. In other words, the strength of the section is not proportional to the section area. According to fracture mechanics, the size effect is relatively small when the member size is small compared to the fracture process zone (Bazant and Planas 1997). When the member size becomes infinite, the strength decreases in proportion to the square root of the size based on linear fracture mechanics as defined in Eq. (5a), and in case of dissimilar cracking, the size effect converges toward a certain value as shown in Eq. (5b).

$$s_e = \frac{1}{\sqrt{1+\alpha_1 d}} \tag{5a}$$

$$s_e = \frac{\alpha_2}{\sqrt{1+\alpha_1 d}} + (1-\alpha_2) \tag{5b}$$

where s_e is the relative strength, α_1 and α_2 are the empirical constants, and d is the characteristic length. Design codes such as *fib*2010 (Federation Internationale du Beton (fib) 2013) simply use Eq. (6) instead of Eq. (5) because the size of the structural members is ordinarily within a specific range.

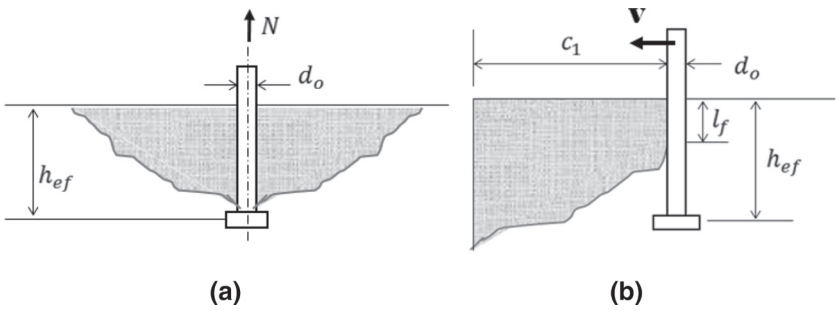

Fig. 5 Size effect on concrete failure due to tensile and shear loading. **a** Concrete cone failure in tension. **b** Concrete breakout failure in shear.

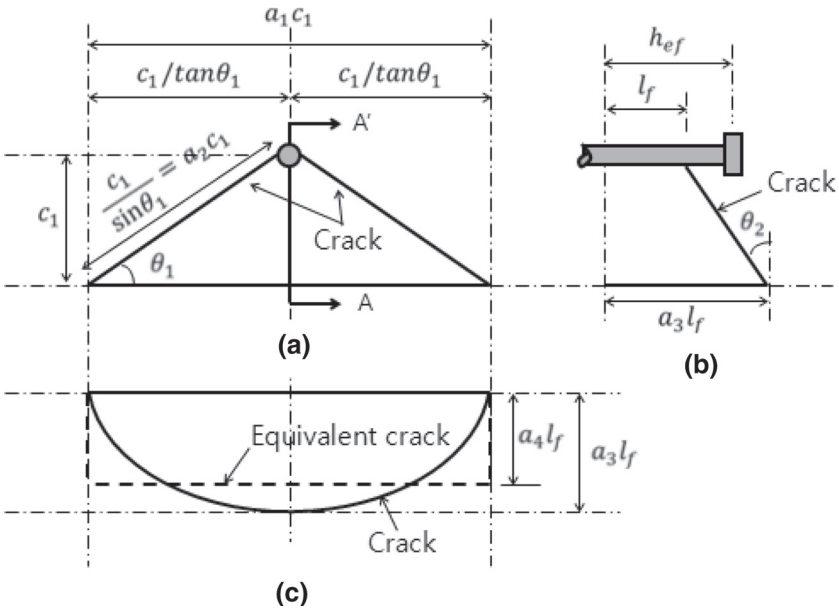

Fig. 6 Failure shape for shear anchor. **a** Plan. **b** Section A–A′. **c** Front view.

$$s_e = \frac{1}{\sqrt[\alpha_3]{d}} \tag{6}$$

where α_3 is an empirical constant ($\alpha_3 \geq 2$).

A comparison between Eq. (5a) and Eq. (6) is shown in Fig. 7. As shown in Fig. 7, if the sizes of the specimens or members are within some range, the size effect can be simply expressed by Eq. (6) rather than Eq. (5). However, Eq. (5) more precisely predicts the size effect than Eq. (6), especially when the sizes of the members are quite different.

The failure area of the anchor for tension and shear is increased as the diameter and its effective embedment depth are increased. In case of the anchor for shear force, the failure area is more complicated than the tension because the failure does not occur through the entire embedment depth h_{ef}. The failure area of both anchors is increased for large anchors, but the resisting strength of the concrete is not proportionally increased due to the size effect. The characteristic length d for the anchor under shear load can be roughly replaced by the edge distance c_1.

3.3 Prying Effect

As shown in Fig. 8, the reaction force P_2 is created near the end of the anchor when the shear force is applied to the anchor. Equation (7) establishes an equilibrium of the force.

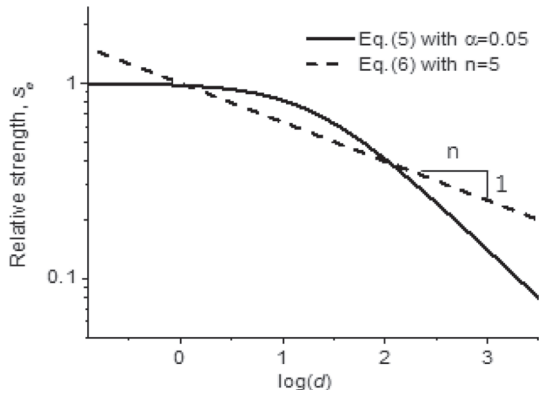

Fig. 7 Size effect based on fracture mechanics.

$$P_2 = \left(\frac{h_1}{h_2}\right) P_1 \tag{7a}$$

$$P_3 = P_1 + P_2 = \left(\frac{h}{h_2}\right) P_1 = m_f P_1 \geq P_1 \tag{7b}$$

where P_1 is the force applied to the anchor, P_2 is the reaction force, P_3 is the resultant force of P_1 and P_2, i.e., the shear force to the concrete, h is the distance between P_1 and P_2, h_1 is the distance between P_1 and P_3, h_2 is the distance between P_2 and P_3, and m_f is load-magnification factor.

The resultant force P_3 induces the breakout failure, which is greater than the externally applied force P_1 as shown in Eq. (7b). The prying effect represents the generation of a reaction force P_3 greater than the externally applied force P_1, and h/h_2 in Eq. (7b) is called the load-magnification factor m_f. This load-magnification factor is related to the equilibrium distance of the reaction forces and these reactions are related to the stress distribution. The stress distribution is affected by the displacement of the anchor, a crack in the concrete and so on. Displacement of the anchor is a function of its flexural rigidity, which is proportional to h_{ef}^3/EI for a concentrated load and h_{ef}^4/EI for a uniformly distributed load. Therefore, the load-magnification factor m_f, depending on the stress distribution due to the prying effect, can be expressed as Eq. (8).

$$m_f = m_{10}\left(\frac{h_{ef}}{d_o}\right)^{m_{11}} d_o^{m_{12}} \tag{8}$$

where m_{10}, m_{11}, and m_{12} are empirical constants.

Elastic analysis for a simple beam with spring supports is conducted to support the prying effect even though concrete is not elastic. In other words, the prying effect in concrete can be predicted through the elastic analysis. A beam used for the analysis has elastic modulus of 200,000 MPa, and the spring constant of the spring support is 20,000 N/mm. A point load is applied at the end of the beam, and reaction force at each support is obtained. One of the analytical results, the reaction force, is as shown in Fig. 8b, c. From this results, P_1, P_2, P_3, and m_f can be found. The resultant

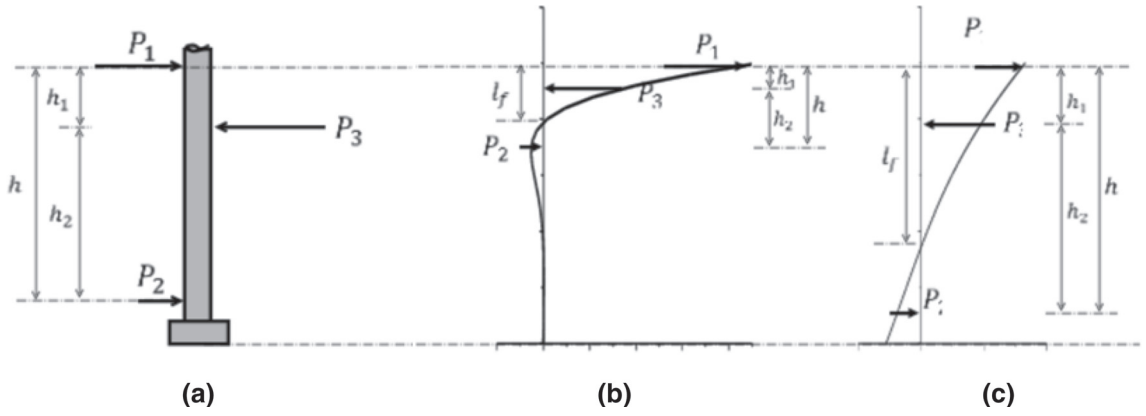

Fig. 8 Prying effect of anchor under shear loading. **a** Reaction for shear. **b** Small anchor. **c** Large anchor.

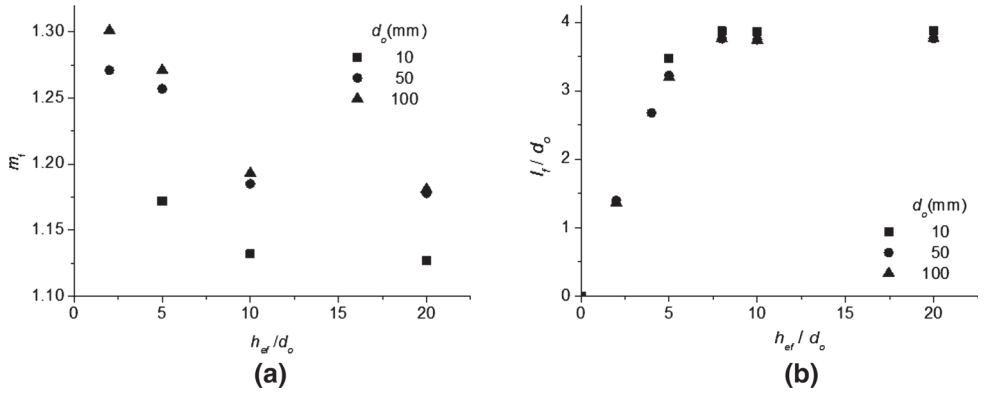

Fig. 9 Load-bearing length and load-amplification factor depending on the embedment depth and diameter of anchor based on the elastic analysis. **a** Load-magnification factor, m_f. **b** Depth of failure, l_f.

P_3 and the distances between the forces are different depending on the size of the anchor, as previously explained.

Load-magnification factor m_f depending on the embedment depth h_{ef} and diameter d_o is presented in Fig. 9a. As shown in Fig. 9a, the load-magnification factor is related with the embedment depth and the diameter which is closely related to flexural rigidity, and it can be explained by Eq. (8). It can be also found that the load-magnification factor has little effect on the load-magnification factor whereas the diameter does when $h_{ef}/d_o \geq 8$. In this case, Eq. (8) can be simplified as Eq. (9).

$$m_f = m_{13} d_o^{m_{14}} \tag{9}$$

where m_{13} and m_{14} are empirical constants.

Figure 9b shows the depth of failure l_f depending on the embedment depth h_{ef} and diameter d_o based on the elastic analysis results. Depth of failure l_f increases with an increase in the embedment depth h_{ef}. Therefore, the depth of failure l_f can be written as Eq. (10) with some empirical constants.

$$l_f = m_{15} \left(\frac{h_{ef}}{d_o} \right)^{m_{16}} d_o \tag{10}$$

where m_{15} and m_{16} are empirical constants.

The failure depth becomes almost constant about 3.8 for $h_{ef}/d_o \geq 8$ in this elastic analysis as shown in Fig. 9b. This result is similar to the experimental result in Fig. 4. The front view of failed large anchors with the condition $h_{ef}/d_o \geq 8$ shows the depth of failure surface as $l_f = 4d_o$ in Fig. 4.

3.4 Derivation of New Model Equations for Breakout Shear Strength with Consideration of the Size Effect and the Prying Effect

As shown in Table 3, the existing prediction equations in ACI 349 (2015) do largely overestimate the shear strength for large size anchors, while the equations predict with a safety margin the shear strength for small size anchors. Therefore, it is necessary to develop a new prediction equation by considering the size effect and the prying effect, and also including the test results for large size anchors.

The concrete strength for the breakout failure of an anchor under shear load can be defined as Eq. (11) based on the failure area, size effect and prying effect. In other words, Eq. (11) is composed of Eqs. (3) or (4) for the failure area, concrete strength f_{ck}, Eqs. (5a) or (6) for size effect, and the load-magnification factor in Eqs. (8) or (9) for the prying effect.

$$V_b = m_{17} \left(A_f f_{ck}^{m_{18}} \right) \times s_e / m_f \tag{11}$$

where m_{17} and m_{18} are empirical constants.

This equation, Eq. (11) can be divided into four types depending on the decision of the failure area A_f and the relative strength s_e as in the following Eq. (12).

$$\begin{aligned} V_b &= m_1 c_1 \left(c_1 + m_3 \left(\frac{l_f}{d_o} \right)^{m_4} d_o^{m_5} \right) f_{ck}^{m_{18}} \times \frac{1}{\sqrt{1+\alpha_1 c_1}} \\ &\quad \times \frac{1}{m_{13} d_o^{m_{14}}} \\ &= n_1 \left(c_1 + n_2 l_f^{n_4} d_o^{n_5} \right) f_{ck}^{n_6} \frac{c_1}{\sqrt{1+n_3 c_1}} \frac{1}{d_o^{n_8}} \end{aligned} \tag{12a}$$

$$\begin{aligned} V_b &= m_1 c_1 \left(c_1 + m_3 \left(\frac{l_f}{d_o} \right)^{m_4} d_o^{m_5} \right) f_{ck}^{m_{18}} \times \frac{1}{c_1^{1/\alpha_3}} \times \frac{1}{m_{13} d_o^{m_{14}}} \\ &= n_1 \left(c_1 + n_2 l_f^{n_4} d_o^{n_5} \right) f_{ck}^{n_6} c_1^{n_7} \frac{1}{d_o^{n_8}} \end{aligned} \tag{12b}$$

$$\begin{aligned} V_b &= m_6 \left(\frac{l_f}{d_o} \right)^{m_7} d_o^{m_8} f_{ck}^{m_{18}} c_1^{m_9} \times \frac{1}{\sqrt{1+\alpha_1 c_1}} \times \frac{1}{m_{13} d_o^{m_{14}}} \\ &= n_1 l_f^{n_4} d_o^{n_5} f_{ck}^{n_6} \frac{c_1^{n_7}}{\sqrt{1+n_3 c_1}} \end{aligned} \tag{12c}$$

$$\begin{aligned} V_b &= m_6 \left(\frac{l_f}{d_o} \right)^{m_7} d_o^{m_8} f_{ck}^{m_{18}} c_1^{m_9} \times \frac{1}{c_1^{1/\alpha_3}} \times \frac{1}{m_{13} d_o^{m_{14}}} \\ &= n_1 l_f^{n_4} d_o^{n_5} f_{ck}^{n_6} c_1^{n_7} \end{aligned} \tag{12d}$$

where n_1, n_2, n_3, n_4, n_5, n_6, and n_7 are empirical constants that can be defined by a regression analysis of the experimental results and the results from the literature.

For load-magnification factor m_f in Eq. (9) is used for the final prediction equation in order to make the equation

simple and most of the experimental results are within the range of $h_{ef}/d_o \geq 8$. Although Eq. (10) is suggested through the elastic analyses, the actual depth of failure of the anchor is not exactly the same as in the analysis. Furthermore, the calculation of the depth of failure for every anchor is not practically appropriate. Therefore, the depth of failure l_f is substituted for the model equations as the same as l_e in the ACI model equations in which $l_e = h_{ef}$ for anchors with a constant stiffness over the full length of an embedded section, and l_e will never exceed $8d_o$ (ACI Committee 349 2015), and empirical constants are found within this condition.

4. Suggestion of New Model Equations for Breakout Shear Strength of Anchors

4.1 Regression Analysis of Experimental Results for the Derived New Models

Regression analysis for identification of Eq. (12) is conducted by using not only the experimental results for large anchors but also the results for small anchors from the literature (Bailey and Burdett 1977; Klingner and Mendonca 1982; Hallowell 1996; McMackin et al. 1973; Klingner et al. 1982, 1999; Swirsky et al. 1977; Ollgaard et al. 1971; Korea Concrete Institute (KCI) 2012). For the regression analysis, however, it is necessary to accommodate some limitation because some values must have some limitations for physical phenomena. In addition, the exponent of compressive strength by regression analysis is fixed to be the same as the current value 0.5 ($n_6 = 0.5$) to maintain the form of the current equation as much as possible and to represent the tensile strength of the concrete. The exponent n_8 for considering the load-magnification factor is fixed as 0.034 ($n_8 = 0.034$), which is from the regression of m_f by Eq. (9). This fixation of parameters does not considerably change the coefficient of determination (R^2) of the regression analysis. The final empirical constants by the regression analysis are shown in Table 4.

4.2 Suggestion of the New Model Equations

In this paper, the most sophisticated and simplest equation among all the types of Eq. (12), Eqs. (12a) and (12d), are finally suggested to predict the breakout shear strength of anchors because it is practically hard to use all the types of Eq. (12). Regression analysis is conducted again to reduce the significant figure of constants in Table 4 by fixing the exponents n_i (i = natural number) rounded off and finding the coefficients n_i (i = natural number) one by one. The final model equations are the following types of Eq. (13).

$$V_b = 0.36\left(c_1 + 10d_o^{0.64}\right)f_{ck}^{0.5}\frac{c_1}{\sqrt{1+0.001c_1}}\frac{1}{d_o^{0.034}} \tag{13a}$$

$$V_b = 2.3d_o^{0.13}f_{ck}^{0.5}c_1^{1.6} \tag{13b}$$

Equation (13b) is directly comparable with the ACI model because both have the same format. The exponent of diameter d_o is decreased in Eq. (13b) compared to the ACI model because it includes the experimental results of large anchors that have a prying effect that is larger than that in small anchors. The exponent of edge distance c_1 in Eq. (13b) is similar to the ACI model even though the ACI model does not explicitly include the size effect. However, the effect of the load-bearing length is disregarded in Eq. (13) by regression because load-bearing lengths of large anchors by experiment become identical by the upper limit 8 d_o because the embedment depths of large anchors are deep enough. In addition, every embedment depth h_{ef} of data used for the regression is over $3.5 \times d_o$, and the load-bearing length does not change significantly on this condition as shown in Fig. 9b. This fact also leads to the neglect of the load-bearing length in Eq. (13).

A comparison between the prediction by each type of Eq. (13) and the test results is included in Fig. 10. Improvement of the suggested Eq. (13) can be seen in Fig. 11, which represents the ratio of the experimental results to the prediction by the equations according to the diameter of the anchor. The ACI model overestimates the shear strength of large size anchors as shown in Fig. 11a. The average ratio between the test and the prediction by the

Table 4 Exponents of Eq. (13).

No.	Limit	Equation (13a)	Equation (13b)
n_1	≥ 0	0.365	1.052
n_2		10.0	5.0
n_3		0.001	–
m_1		0	0
m_2		0.636	0.751
m_3		0.5	
m_4		–	0.798
m_5		0.034	
R^2		0.954	0.957

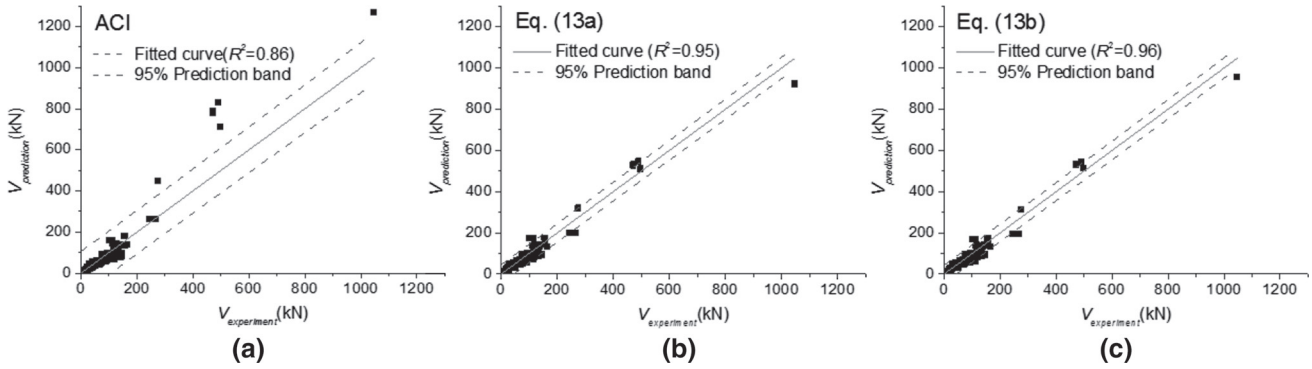

Fig. 10 Comparison of experimental results and predictions. **a** ACI, **b** Eq. (13a), **c** Eq. (13b).

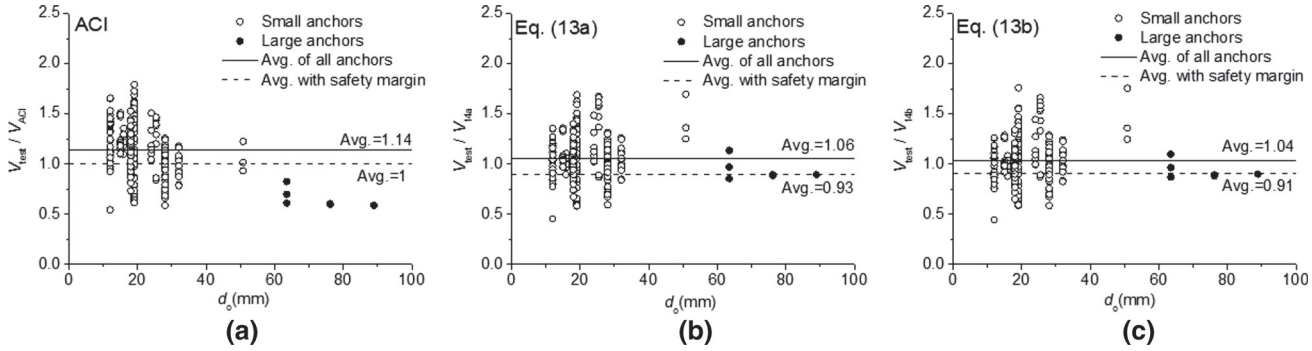

Fig. 11 Ratio of experimental results to prediction. **a** Prediction by ACI model. **b** Prediction by Eq. (13a). **c** Prediction by Eq. (13b).

ACI model for anchors with small diameters of less than 50 mm is about 1.14 and it reveals that the safety margin of ACI is about 14 %. Overestimated cases are located under the dashed line in Figs. 11b and c in which the safety margin is fixed as the same as the ACI model. The suggested models reduce the portion of the overestimation, which is dangerous for the structures. In conclusion, both proposed equations are more reliable and improve the prediction for large anchors compared to the current ACI model.

5. Conclusion

The main conclusions are as follows.

(1) Experiments are conducted to verify the effect of the diameter, embedment length and edge distance. Experimental results show that the existing models overestimate the shear strength of large anchors.

(2) New model equations for prediction of breakout shear strength of anchors, including large size anchors, based on the theoretical background such as the failure surface, prying effect and size effect are suggested through experiments and regression analysis. Elastic analyses are conducted to identify the prying effect of anchors and the results confirm that magnification of load due to the prying effect increases along with an increase in anchor size. The size effect is also considered with two types of equation.

(3) Consideration of both the prying effect and the size effect is more significant for large size anchors than regular size anchors.

(4) Two types of model equations are finally suggested. The suggested equations reduce the overestimation and reliably predict shear breakout strength of anchors.

Open Access

References

ACI Committee 318. (2015). *Building code requirements for structural concrete (ACI 318)*, Farmington Hills, MI.

ACI Committee 349. (2015). *Code requirements for nuclear safety related concrete structures (ACI 349-13)*, Farmington Hills, MI.

Arkansas Nuclear One Steam Electric Station. (1992). Arkansas nuclear one maxibolt anchor bolt test program, entergy operations. MCS Design

ASTM A 540. (2005). *Standard specification for alloy–steel bolting materials for special applications: Class B*.

ASTM E 488-98. (1998). *Standard test methods for strength of anchors in concrete and masonry elements*.

Bailey, J. W., & Burdett, E. G. (1977). Edge effects on anchorage to concrete. *Civil Engineering Research Series, 31*, 120.

Bazant, Z. P., & Planas, J. (1997). *Fracture and size effect in concrete and other quasibrittle materials*. Boca Raton, LA: CRC Press.

Federation Internationale du Beton (fib). (2013). *fib model code for concrete structures 2010*. Berlin, Germany: Ernst & Sohn.

Fuchs, W., Eligehausen, R., & Breen, J. (1995). Concrete capacity design (CCD) approach for fastenings to concrete. *ACI Structural Journal, 92*(6), 794–802.

Hallowell, J. (1996). Tensile and shear behavior of anchors in uncracked and cracked concrete under static and dynamic loading. M.S. Thesis, The University of Texas at Austin.

Klingner, R. E., & Mendonca, J. A. (1982). Shear capacity of short anchor bolts and welded studs: A literature review. *Journal of the American Concrete Institute, 79*(5), 339–349.

Klingner, R., Mendonca, J., & Malik, J. (1982). Effect of reinforcing details on the shear resistance of short anchor bolts under reversed cyclic loading. *ACI Journal, 79*(1), 3–12.

Klingner, R. E., Muratli, H., & Shirvani, M. (1999). A technical basis for revision to anchorage criteria, NUREG/CR-5563.

Korea Concrete Institute (KCI). (2012). *Concrete design code; Design guidline for anchoring to concrete*.

KS F 2405. (2010). *Standard test method for compressive strength of concrete*.

Lee, N. H., Park, K. R., & Suh, Y. P. (2010). Shear behavior of headed anchors with large diameters and deep embedments. *ACI Structural Journal, 107*(S14), 146–156.

McMackin, P., Slutter, R., & Fisher, J. (1973). Headed steel anchors under combined loading. *AISC Engineering Journal, 10*(2), 43–52.

Ollgaard, J., Slutter, R., & Fisher, J. (1971). Shear strength of stud connectors in lightweight and normal weight concrete. *AISC Engineering Journal, 8*(2), 55–64.

Swirsky, R., Dusel, J., Crozier, W., Stoker, J., & Nordlin, E. (1977). Lateral resistance of anchor bolts installed in concrete, report no. FHWA-CA-ST-4167-77-12. California Department of Transportation, Sacramento, CA.